

Laboratory spectra of CO₂ vibrational modes in planetary ice analogs

Douglas W. White^{a,*}, Rachel M.E. Mastrapa^b, Scott A. Sandford^a

^aNASA Ames Research Center, Moffett Field, CA 94035, USA

^bThe SETI Institute, Mountain View, CA 94035, USA

ARTICLE INFO

Article history:

Received 8 August 2012

Revised 4 October 2012

Accepted 5 October 2012

Available online 1 November 2012

Keywords:

Ices, IR spectroscopy
Experimental techniques
Organic chemistry
Satellites, Surfaces

ABSTRACT

Laboratory spectra have shown that CO₂ is a powerful diagnostic tool for analyzing infrared data from remote observations, as it has been detected on icy moons in the outer Solar System as well as dust grain surfaces in the interstellar medium (ISM). IR absorption band profiles of CO₂ within ice mixtures containing H₂O and CH₃OH change with respect to temperature and mixture ratios. In this particular study, the ν_3 CO₂ asymmetric stretch mode near 4.3 μm (2350 cm^{-1}), overtone mode near 1.97 μm (5080 cm^{-1}), and the combination bands near 2.7 μm (3700 cm^{-1}), 2.8 μm (3600 cm^{-1}), and 2.02 μm (4960 cm^{-1}), are systematically observed in different mixtures with H₂O and CH₃OH in temperature ranges from 15 K to 150 K. Additionally, some high-temperature deposits ($T > 50$ K) of H₂O, CH₃OH, and CO₂ ice mixtures were performed and it was discovered that CO₂ may deposit out at higher temperatures than previously recorded. These data may then be used to interpret infrared observational data obtained from icy surfaces in the outer Solar System and beyond.

© 2012 Elsevier Inc. All rights reserved.

1. Introduction

Icy materials in dense clouds in the interstellar medium (ISM) are observed by the absorption of starlight through these clouds (e.g., Chiar et al., 1995). Such ices are typically dominated by H₂O-ice in an amorphous phase, or amorphous solid water (ASW) and often contain other simple species like CO, CO₂, CH₃OH, and NH₃ (e.g., Jenniskens et al., 1995; Lacy et al., 1998; Ehrenfreund et al., 1999; Gibb et al., 2000; Herbst, 2001). Infrared (IR) absorption spectroscopy in the near-IR ($\lambda = \sim 0.9\text{--}2.5$ μm) and mid-IR ($\lambda = 2.5\text{--}25$ μm) are powerful methods by which these icy components can be detected and studied. IR absorption band positions and profiles are used for identification of physical properties such as composition, and temperature Allamandola et al. (1992), Salama et al. (1994), Chiar et al. (1995), Ehrenfreund et al. (1999), Gerakines et al. (1999), Gibb et al. (2000), Bernstein et al. (2005), White et al. (2009), and Öberg et al. (2009). Temperatures of H₂O-dominated ice mixtures can range from 10 to 15 K in quiescent interstellar dust cloud environments to as high as 100–150 K around protostellar disks.

The properties of icy materials in the Solar System and dense clouds in the ISM are typically observed using infrared absorption features from transmitted or reflected light on icy surfaces (e.g., Ehrenfreund, 1999; Dartois et al., 1999; Sandford et al., 2001; Grundy et al., 2006; Cruikshank et al., 2010). Ices on planetary surfaces in the outer Solar System are commonly also dominated by

H₂O (Fink et al., 1976; Jenniskens and Blake, 1996; Dartois and Schmitt, 2009; Cruikshank et al., 2010). Observations from instruments such as the Visual and Infrared Mapping Spectrometer (VIMS) instrument aboard the Cassini spacecraft have revealed that most of the H₂O-ice on outer Solar System surfaces, specifically jovian and saturnian satellites, is of crystalline phase (e.g., Cruikshank et al., 2010). As in ISM ices, additional compounds are often present in these H₂O-dominated ices (e.g., Grundy et al., 1999; Cruikshank et al., 2010). For example, spectroscopic data from the Near-infrared mapping spectrometer (NIMS) aboard the Galileo spacecraft that explored satellites such as Ganymede and Callisto indicated the presence of CO₂ within the host ice (Carlson et al., 1996; McCord et al., 1998; Hibbitts et al., 2000, 2002, 2003; Cruikshank et al., 2010). Temperatures of H₂O-dominated ice mixtures typically found on outer Solar System surfaces typically range from 50 to 160 K. These temperatures can vary with time and location, depending on sunlight exposure, local geological activity, etc.

CO₂ is important in studies of icy surfaces on planetary bodies in the Solar System because the IR absorption profiles of CO₂-containing ices created in the laboratory have been shown to be sensitive to conditions of the ice such as temperature, temperature history, ice composition, and radiation exposure (Sandford and Allamandola, 1990a; Ehrenfreund et al., 1998, 1999; Gerakines et al., 1999; Dartois et al., 1999; Moore et al., 2001; Hudson and Moore, 2000, 2001; van Broekhuizen et al., 2006; Hodyss et al., 2008; White et al., 2009; Öberg et al., 2007, 2009). These investigations provide a relevant database indispensable to spectral analysis from remote measurements (e.g., Sandford and Allamandola, 1990a;

* Corresponding author.

E-mail address: douglas.white@nasa.gov (D.W. White).

Ehrenfreund et al., 1998; Gálvez et al., 2007; Gerakines et al., 2005; Cook et al., 2011). Use of laboratory techniques by Hudgins et al. (1993), Bernstein et al. (1995), and Ehrenfreund et al. (1996), for example, allowed study of the molecular compositions and interactions of materials such as CO₂ within H₂O–ice structures in interstellar environments via IR absorption spectroscopy. However there remain many variations of mixture, temperature, and compositions of CO₂-containing ices relevant to ices in the ISM and outer Solar System that have not yet been examined, particularly H₂O-rich ices that contain CH₃OH.

H₂O–ice undergoes several phase changes as it is warmed from its amorphous phase a 10 K to its sublimation temperature (e.g., Tielens and Hagen, 1982; Smith, 2000; Baragiola, 2003). These changes can be observed via IR absorption spectroscopy. H₂O-rich ices that contain other molecules can also undergo phase transitions. For example, Öberg et al. (2009) have shown that H₂O + CO₂ ice mixtures undergo both surface and bulk segregation induced by thermal annealing, as observable through reflection–absorption infrared spectroscopy (RAIRS). As another example, thermal processing of H₂O–CH₃OH ices can spontaneously form clathrate hydrates that can trap volatiles such as CO₂ (Blake et al., 1991; Dartois and Schmitt, 2009). The impurity in the H₂O–ice cage may desorb into the ice matrix as the sample is heated (Hornekaer et al., 2005). Also, warming the ice leads to segregation of the H₂O component from CH₃OH in H₂O–CH₃OH mixtures causing H₂O crystals and CH₃OH crystals to form in separate regions (Blake et al., 1991; Tielens, 2005). Trapped volatiles may begin to escape from a H₂O–ice mixture around 75 K due to pore collapse as it is heated, though some of the trapped species may still remain. Above 120 K, a “glass transition” occurs and the remaining pores collapse until ~140 K when the crystalline H₂O structure transitions to a cubic phase, and there is a sudden release of the trapped species near 150 K. The glass transition precedes crystallization of an amorphous material and represents the temperature at which the molecules can begin to migrate more rapidly. Upon heating the amorphous phase ice, the onset of structural relaxation occurs between 120 and 142 K, depending on the heating rate and time since deposition (Jenniskens and Blake, 1996). Reorganization of the surface leads to collapse of the pores and reduction in the number of dangling OH bonds (Cyriac and Pradeep, 2008). Jenniskens and Blake (1996) interpreted the onset of the glass transition as a transformation to a new phase. In this phase, the increasing temperature allows the relaxation of the structure and removes strained bonding angles. Recent calorimetry experiments question whether the glass transition is even detectable (Yue and Angell, 2004). Although, other measurements confirmed the glass transition at 136 K (Kohl et al., 2000). A detailed review of glass transition in pure and aqueous solutions, can be found in Angell (2002).

In the new laboratory study described here, the IR spectra of ices bearing H₂O, CH₃OH, and CO₂ have been measured while systematically varying mixture ratios and temperatures that span the range of values expected on icy surfaces in the outer Solar System as well as the ISM. The experiments in this study also investigate the CO₂ absorptions from some binary and ternary ice mixtures in order to expand upon the existing databases and further facilitate understanding of observations from ground- and space-based instruments.

2. Experiments

2.1. Apparatus

The apparatus used for this study has been described in Hudgins et al. (1993), Bernstein et al. (2006), and Mastrapa et al. (2008). A high vacuum (~1 × 10⁻⁷ mbar) simulation chamber

was placed within the sample compartment of a Bio Rad Excalibur FTIR Spectrometer with a spectral range of 0.910–22.2 μm (11,000–450 cm⁻¹) and a spectral resolution of 1 cm⁻¹. The multiple-windowed vacuum chamber has IR-transparent KBr windows and houses a ZnSe substrate (window) that is attached to a water-cooled closed-cycle He cryocooler (Air Products Displex IRO2W) that can be cooled to temperatures as low as 15 K. The ZnSe substrate can be rotated within the sample chamber without breaking vacuum. The chamber houses four ports consisting of KBr windows through which the IR beam was sent and a UV transparent window for UV photolysis (not used in this study). The stainless steel vacuum chamber was evacuated using an oil diffusion pump (Edwards Diffstack Series 100) backed by a mechanical pump (Edwards E2M5). The temperature of the ZnSe window was controlled using a small resistive heater mounted on the cold finger just above the substrate and monitored with two Fe–Au/chromel thermocouples attached to the heater and sample holder. A temperature controller (Scientific Instruments 9650) was used to monitor and control sample temperatures. A diaphragm gauge was used on the system to measure sample bulb pressure, while thermocouple and ion gauges allowed constant monitoring of the pressure inside the vacuum chamber. To measure sample thickness, a HeNe laser (λ = 0.633 μm) was used with a photometer to count interference fringes as the ice was deposited (see Section 2.2).

2.2. Experimental procedure

Gases were mixed in glass bulbs using a separate greaseless glass manifold at room temperature using the same method as e.g., Hudgins et al. (1993). Ambient pressures in the manifold were typically ~5 × 10⁻⁶ T and bulb pressures after preparation were typically ~19 T. Thus contaminants were limited to about one part in 4 × 10⁶. After the gas mixtures were prepared, the bulb was then mounted onto the cryocooler apparatus.

The sample substrate in the cryovacuum system was cooled to the deposition temperature (15 or 50 K for most samples) and a background absorption spectrum was taken of the blank sample substrate. The gas mixture was then vapor-deposited onto the substrate, typically at a rate of about 0.1 μm min⁻¹. Sample thickness is calculated using the equation

$$d = m\lambda_0 / (2n_{ice} \cos \theta_{ice}), \quad (1)$$

where d is the thickness of the ice in μm, m is the number of fringes observed in the laser light during deposition, λ_0 is the laser wavelength (0.633 μm), n_{ice} is the index of refraction of the ice [1.32 for crystalline H₂O–ice (Hale and Querry, 1973), 1.29 for amorphous H₂O–ice (Westley et al., 1998; Dohnálek et al., 2003)], and θ_{ice} is the angle of reflection in the ice (taken to be 45°). After the ice was fully deposited, its spectrum was obtained and ratioed to the background spectrum.

In many cases, the ices were subsequently warmed, or warmed and cooled, and additional spectra were taken at higher temperatures. Temperatures where spectra were measured were selected based on where ice segregation is known to occur (e.g., Blake et al., 1991; Jenniskens and Blake, 1996; Ehrenfreund et al., 1997, 1999; Gerakines et al., 1999). The temperature of the sample window inside the chamber was adjusted from 15 K up to 170 K at a rate of 2 K min⁻¹ and cooled at a rate of ~10 K min⁻¹ in order to observe effects on the ice sample when the temperature is cycled. Samples were held at temperature while absorption spectra were collected. Warming often causes significant changes in the spectra of ices as molecules rearrange and warming rates faster than 2 K min⁻¹ can cause sudden loss of material. However, the cooling rate was not observed to make much difference in the spectral profiles. Thus a faster cooling rate was used. The CO₂ spectra typically reflect the highest temperature at which the ice has been if the

sample was heated (see Section 3). In some experiments involving mostly H₂O (where the ice is >60% H₂O), samples were deposited at 50 K to reduce the effect of scattering seen in low-temperature amorphous samples deposited at 15 K.

2.3. Ice compositions

The ice compositions and temperatures investigated in this study are summarized in Table 1. The mid-IR spectra, $\lambda = 2.5\text{--}22\ \mu\text{m}$ ($7500\text{--}450\ \text{cm}^{-1}$), were measured for several different ice compositions at temperatures ranging from 15 to 150 K. In addition, spectra in the range $\lambda = 0.9\text{--}3.5\ \mu\text{m}$ ($11,000\text{--}2850\ \text{cm}^{-1}$) were studied to identify temperature and mixture ratio effects on the CO₂ combination and overtone bands for comparison to previous results of mixtures of H₂O + CO₂ and CH₃OH + CO₂ (Bernstein et al., 2005). Thinner samples ($\sim 0.2\text{--}2\ \mu\text{m}$) were needed for mid-IR experiments so the asymmetric stretch mode of CO₂ was not saturated. Conversely, thicker samples ($\sim 2\text{--}4\ \mu\text{m}$) were used in near-IR experiments in order to view the much weaker combination

Table 1
Ice mixtures, ratios, and vibrational modes observed in this study.

Mixture and temperature	Assignments ^a	Position [μm (cm^{-1})]
H ₂ O + CO ₂ 24:1 ^b at 15 K	ν_3	4.270 (2342)
	ν_2	15.27 (655.0)
20:1 at 50 K	$\nu_1 + 2\nu_2 + \nu_3$	2.017 (4958)
	$\nu_1 + \nu_3$	2.703 (3700)
	$2\nu_2 + \nu_3$	2.784 (3592)
	ν_3	4.270 (2342)
	ν_2	15.27 (655.0)
CH ₃ OH + CO ₂ 5:1 at 15 K	$2\nu_1 + \nu_3$	1.972 (5072)
	$\nu_1 + 2\nu_2 + \nu_3$	2.019 (4952)
	$4\nu_2 + \nu_3$	2.061 (4853)
	$\nu_1 + \nu_3$	2.704 (3698)
	$2\nu_2 + \nu_3$	2.789 (3585)
	ν_3	4.275 (2339)
	ν_2	15.43 (648.0)
H ₂ O + CH ₃ OH + CO ₂ 10:10:1 ^b at 50 K	ν_3	4.274 (2340)
	ν_2	15.43 (648)
2.2:1.5:1 ^b at 15 K (UAB)	ν_3	4.270 (2342)
	ν_2	15.29 (654.0)
10:1:1 at 50 K	$2\nu_1 + \nu_3$	1.970 (5077)
	$\nu_1 + 2\nu_2 + \nu_3$	2.017 (4958)
	$\nu_1 + \nu_3$	2.702 (3701)
	$2\nu_2 + \nu_3$	2.784 (3592)
	ν_3	4.272 (2341)
	ν_2	15.27 (655.0)
	ν_3	4.272 (2341)
100:1:1 ^b at 50 K	ν_3	4.272 (2341)
	ν_2	15.38 (650.0)
100:50:1 ^b at 50 K	ν_3	4.272 (2341)
	ν_2	15.38 (650.0)
5.3:8.8:1 ^b at 15 K (UAB)	ν_3	4.272 (2341)
	ν_2	15.38 (650.0)
1:10:1 at 15 K	$2\nu_1 + \nu_3$	1.974 (5067)
	$\nu_1 + 2\nu_2 + \nu_3$	2.021 (4947)
	$\nu_1 + \nu_3$	2.706 (3695)
	$2\nu_2 + \nu_3$	2.792 (3582)
	ν_3	4.274 (2340)
	ν_2	15.38 (650.0)
	ν_3	4.274 (2340)
1:1:1 at 50 K	$2\nu_1 + \nu_3$	1.969 (5080)
	$\nu_1 + 2\nu_2 + \nu_3$	2.017 (4959)
	$\nu_1 + \nu_3$	2.703 (3700)
	$2\nu_2 + \nu_3$	2.784 (3592)
	ν_3	4.274 (2340)
	ν_2	15.20 (658.0)
	ν_3	4.274 (2340)

^a Mode assignments from Quirico and Schmitt (1997), Sandford and Allamandola (1990a), and Bernstein et al. (2005). Positions of the modes noted are from when the mixture was deposited. In mixtures where H₂O:CO₂ was 50:1 or more, the ν_2 CO₂ mode was too weak to be seen.

^b Only mid-IR spectra were recorded in this experiment.

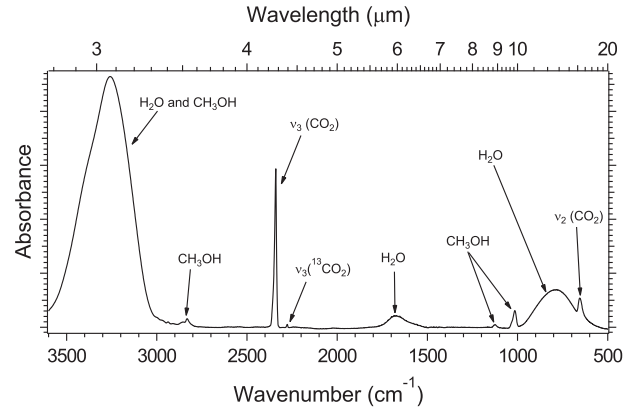


Fig. 1. Mid-IR spectrum of a mixture of H₂O + CH₃OH + CO₂ (10:1:1) deposited at 50 K about 0.35 μm thick.

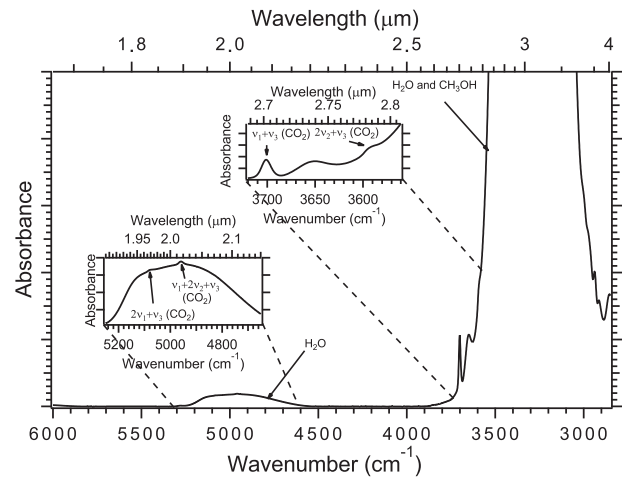


Fig. 2. Near-IR spectrum of a mixture of H₂O + CH₃OH + CO₂ (10:1:1) deposited at 50 K about 2.1 μm thick. The combination and overtone modes of CO₂ are expanded and labeled in the insets.

and overtone modes. Some spectra were collected at the University of Alabama at Birmingham (UAB) Astrophysics Laboratory¹ and are shown here for comparison. Experimental methods and related experiments from UAB are covered in more depth by White et al. (2009) and White (2010).

3. Results

The next subsections contain descriptions of the changes in the asymmetric CO₂ stretch mode [ν_3 , around $4.263\ \mu\text{m}$ ($2346\ \text{cm}^{-1}$) for pure CO₂], and the combination and overtone modes of CO₂ in the near-IR (Table 1). The mid-IR and near-IR spectra of H₂O + CH₃OH + CO₂ (10:1:1) in Figs. 1 and 2 provide examples of the IR bands produced by the different species considered in this paper the absorptions of the different species. It should be noted that, in general, the positions of the CO₂ absorption features undergo irreversible changes as the samples were heated and weakened at temperatures above 100 K where sublimation losses begin to occur.

3.1. The asymmetric CO₂ stretch mode

Several ice mixtures of H₂O, CH₃OH, and CO₂ were heated and cooled in order to examine the behavior of the asymmetric CO₂

¹ <http://www.phy.uab.edu/labastro/>.

stretch mode. Fig. 3 contains plots of CO₂ stretch mode peak position versus temperature for several mixtures. This absorption split into two peaks in some mixtures above 100 K due to increased mobility of the molecules with temperature and population of CO₂ molecules within pores of the ice matrix. Only the position of the stronger low-wavenumber/high-wavelength peaks are noted here for clarity. The implications are discussed in the next section.

3.1.1. H₂O-rich mixtures

We first discuss the changes in the band in H₂O-dominated ices (mixtures with >50% H₂O), since absorption profiles were similar in temperature and appearance in H₂O-rich mixtures containing H₂O, CH₃OH, and CO₂. Samples were deposited at a low temperature (15 or 50 K) and heated 2 K min⁻¹ before cooling. For these H₂O-rich samples, the CO₂ stretch mode would start out near 4.274 μm (2340 cm⁻¹) and shift by as much as 0.01 μm (4 cm⁻¹) to a higher wavelength as the sample was heated to and above 150 K and cooled (e.g., Fig. 3). In most cases, the changes in band positions were irreversible. However, in mixtures of H₂O + CO₂ where H₂O comprised more than 66% of the mixture, the CO₂ stretch mode position could shift back to previous positions during a heating and cooling cycle within the range 70–120 K (Fig. 3—only one heating/cooling cycle is shown here).

An example of CO₂ stretch mode profiles in a H₂O-dominated mixture [H₂O + CH₃OH + CO₂ (10:1:1)] is shown in Fig. 4. A single peak at 4.272 μm (2341 cm⁻¹) is seen in the ice mixture after deposition at 50 K. A second peak appears near 4.263 μm (2346 cm⁻¹) when heating between 130 and 140 K, a change only seen in mixtures with >66% H₂O. The peak near 4.263 μm (2346 cm⁻¹) shifts back to 4.274 μm (2340 cm⁻¹) above 160 K as the CO₂ sublimates. Between 120 and 140 K, the long wavenumber peak would often intensify as the shorter wavenumber peak would diminish. However, it was generally observed that in H₂O-dominated mixtures, the greater the proportion of H₂O to CO₂, the less likely that more than one peak would appear in the CO₂ asymmetric stretch mode profiles as the temperature increased. This is probably because at lower concentrations of CO₂ molecules in the ice, individual molecules are more fully isolated from one another.

3.1.2. CH₃OH-rich mixtures

Here we discuss CH₃OH-dominated mixtures (mixtures with >50% CH₃OH), all deposited at 15 K and warmed at a rate of 2 K min⁻¹. Absorption profiles of CO₂ were similar to each other in

binary mixtures of CH₃OH and CO₂ so a mixture of CH₃OH + CO₂ (5:1) is discussed as an example. The position of the ν₃ asymmetric stretch mode of the CO₂ maximum changed when the sample was cooled as well as when it was heated. Above 100 K, a broad shoulder appeared near 4.248 μm (2354 cm⁻¹) (Fig. 5). This shoulder remained throughout the cooling process. Re-heating this mixture revealed that the absorbance peak positions retrace some of the positions observed during the first cooling process, although the primary peak near 4.274 μm (2340 cm⁻¹) never returns to its original position at deposition or the first heating process. Absorptions on the ν₃ CO₂ band that appear on the lower wavelength side at higher temperatures (e.g., 130 K) shift towards shorter wavelengths when cooling down as does the peak near 4.275 μm (2339 cm⁻¹). Interestingly, the addition of H₂O to the mixture makes a difference and the spectral behavior of CH₃OH-rich ices of H₂O, CH₃OH, and CO₂ is not similar to that of the CH₃OH + CO₂ ices. In CH₃OH-dominated H₂O + CH₃OH + CO₂ mixtures (1:10:1), the CO₂ stretch mode position only changed by 0.001 μm (1 cm⁻¹) or less during the heating process, and little or no change was seen during cooling (Fig. 3).

3.1.3. Equal mixtures of H₂O and CH₃OH

Though mixtures like H₂O + CH₃OH + CO₂ 1:1:1 and 10:10:1 are not astrophysically relevant, experiments were carried out in order to cover the phase space and understand the interaction of CO₂ with H₂O and CH₃OH (e.g., Ehrenfreund et al., 1999). The position of the asymmetric ν₃ asymmetric stretch mode in mixtures containing equal or nearly equal parts H₂O and CH₃OH was shifted to ~0.002 μm (1 cm⁻¹) longer wavelength than the same feature in H₂O-rich mixtures. In one warm-up experiment of H₂O + CH₃OH + CO₂ (10:10:1), a small peak at 4.30 μm (2323 cm⁻¹) appeared and remained throughout the experiment, as did a similar feature with a H₂O + CH₃OH + CO₂ (1:1:1) mixture at 120 K and remained as the sample was cooled (Fig. 6). It should be noted that the CO₂ profiles in H₂O + CH₃OH + CO₂ (1:1:1) mixtures at the deposition temperature were at the same position as those of the H₂O-rich mixtures. The presence of CH₃OH affects the sample such that this particular vibrational mode will not “backtrack” to a previous position from a warming/cooling cycle as it did in the H₂O + CO₂ (24:1) experiment.

3.1.4. CH₃OH in H₂O + CH₃OH + CO₂ mixtures

The asymmetric C–O stretch mode of CH₃OH appears as a single absorption at deposition at 50 K in these H₂O + CH₃OH + CO₂

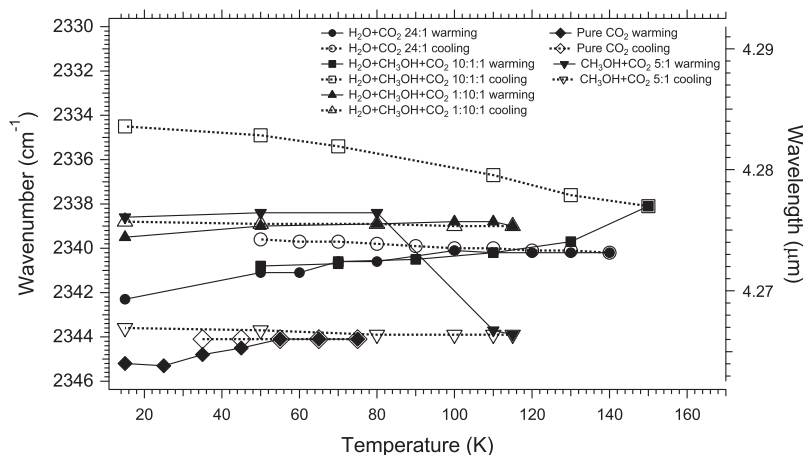


Fig. 3. CO₂ ν₃ asymmetric stretch mode position versus temperature for three mixtures heated at a rate of 2 K min⁻¹ and then cooled. Spectra were taken as the sample was held at the indicated temperature. A plot of pure CO₂ is also shown for comparison. H₂O-dominated ternary mixtures such as H₂O + CH₃OH + CO₂ 10:1:1 and 100:10:1 yielded almost identical stretch mode peak positions so only one representative mixture is shown.

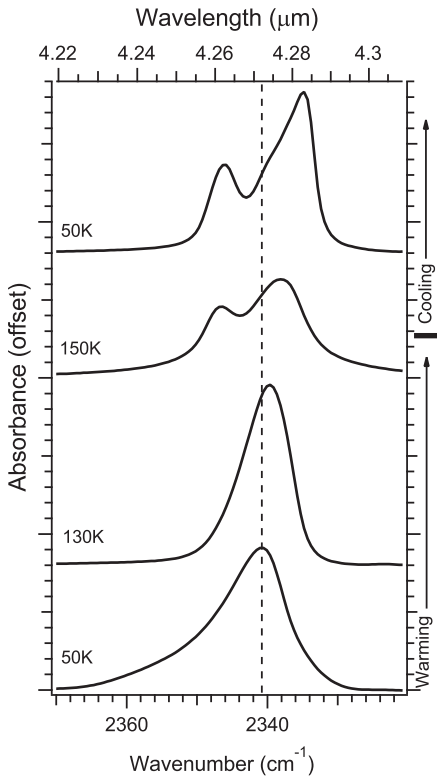


Fig. 4. Selected CO₂ asymmetric stretch mode profiles in a mixture of H₂O + CH₃OH + CO₂ (10:1:1) deposited at 50 K and heated at a rate of 2 K min⁻¹ before cooling down. Spectra were taken while the sample was held at the indicated temperature.

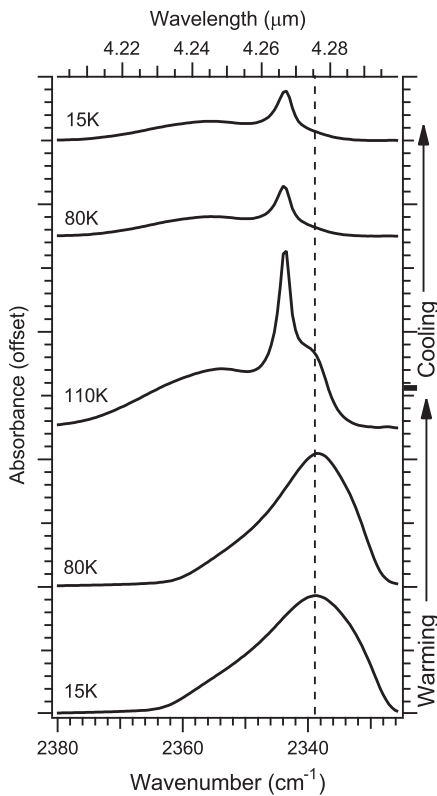


Fig. 5. Selected CO₂ asymmetric stretch mode profiles in a mixture of CH₃OH + CO₂ (5:1) deposited at 15 K, warmed at a rate of 2 K min⁻¹, and cooled down. Spectra were taken as the sample was held at the indicated temperature.

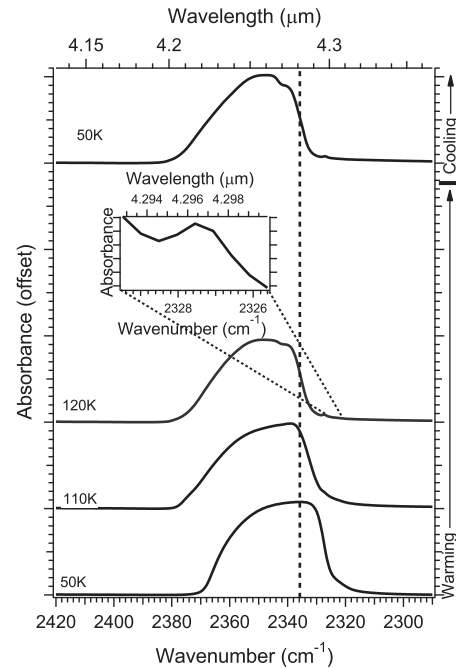


Fig. 6. CO₂ stretch mode profiles in a mixture of H₂O + CH₃OH + CO₂ (1:1:1) deposited at 15 K and heated at a rate of 2 K min⁻¹ to 120 K before cooling down. Spectra were taken as the sample was held at the indicated temperature. The small feature at 2323 cm⁻¹ at 120 K is shown here.

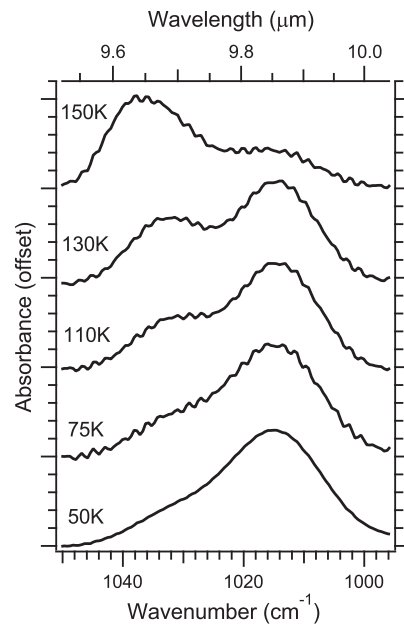


Fig. 7. The asymmetric C–O stretch mode profile of CH₃OH in a mixture of H₂O + CH₃OH + CO₂ (10:1:1) deposited at 50 K and heated at a rate of 2 K min⁻¹. Spectra were taken as the sample was held at the indicated temperature. Spectra became more noisy as the sample was heated.

(10:1:1) mixtures, though a shoulder on the short wavelength side appears as the sample is heated (Fig. 7). This shoulder became stronger than the longer wavelength peak above 110 K. The C–O stretch mode profile of CH₃OH changes with temperature, indicative of the tetrahydrofuran (THF) type II clathrate structure forming from H₂O – CH₃OH complexes (Fleyfel and Devlin, 1991 – see also Section 1).

3.2. Near-IR CO₂ modes

Absorption profiles of mixtures of H₂O, CH₃OH, and CO₂ were also examined in the near-IR. Table 1 contains the combination/overtone modes that were detected in each mixture. Many of the CO₂ overtone and combination modes appeared as broad, weak absorptions superimposed on the side or on top of H₂O and/or CH₃OH absorptions. As a result, many of these features were difficult to analyze due to the relatively strong features of H₂O near 2 μm and 2.95 μm, as well as CH₃OH features near 2.95 μm (in ternary mixtures – see also Fig. 2).

3.2.1. H₂O-rich mixtures

The CO₂ bands produced by H₂O-rich mixtures (mixtures with >50% H₂O) had similar profiles when deposited at low temperatures (15 or 50 K), so a mixture of H₂O + CH₃OH + CO₂ (10:1:1) is discussed here as an example. Fig. 8a–d contains selected spectra of this mixture deposited at 50 K and heated at a rate of 2 K min⁻¹ to 150 K and cooled back down.

The $2\nu_1 + \nu_3$ feature near 1.97 μm (5080 cm⁻¹) appeared as a very weak, broad absorption (less than 5% of the height of the strongest absorption near 2.70 μm) at the deposition temperature. When heating up to 125 K, the peak began to grow sharper (Fig. 8a). This profile continued to become stronger by a factor of 2 up to 150 K and remained throughout the cooling process. While cooling, a broad absorption near 1.972 μm (5070 cm⁻¹) also appeared and became more distinct as the sample was cooled. This absorption is most likely due to the interaction of CO₂ and H₂O (Bernstein et al., 2005). This particular mode was very difficult to isolate because it appears directly on top of a large absorption feature due to H₂O.

The $\nu_1 + 2\nu_2 + \nu_3$ mode appeared near 2.017 μm (4958 cm⁻¹) and at least twice the height of the $2\nu_1 + \nu_3$ absorption at the deposition temperature (50 K). This mode was difficult to detect as it is on the large absorption feature due to H₂O. At 120 K, this absorption changed into a broader peak near 2.018 μm (4956 cm⁻¹) and a smaller “bump” near 2.012 μm (4971 cm⁻¹) (Fig. 8b). The 2.012 cm⁻¹ absorption became sharper (about twice the relative intensity of the 2.018 μm (4956 cm⁻¹) absorption) as the sample was heated to 150 K and remained so even after cooling down to 50 K. The 2.018 μm (4956 cm⁻¹) absorption, however, remained broader (\leq half the intensity of the 2.012 μm feature) when heating to 150 K and shifted to 2.019 μm (4953 cm⁻¹). Interestingly, as the sample was cooled this absorption continued to move to about 2.020 μm (4951 cm⁻¹) and became a sharper peak with about the same height as the 2.012 μm feature and a wing at 2.016 μm (4960 cm⁻¹).

The $\nu_1 + \nu_3$ mode near 2.703 μm (3700 cm⁻¹) remained the strongest CO₂ absorption profile in the spectral range 0.9–3.5 μm (11,000–2850 cm⁻¹) throughout the experiment (Fig. 8c). This absorption shifted to about 2.704 μm (3698 cm⁻¹) as the sample was heated, and at 125 K a second peak appeared at 2.697 μm (3708 cm⁻¹). This new peak became the dominating absorption profile at 140 K. At 150 K, a third peak appeared in between these two at 2.700 μm (3704 cm⁻¹) as the 2.704 μm (3698 cm⁻¹) peak shifted to 2.706 μm (3695 cm⁻¹) and the peak at 2.697 μm (3708 cm⁻¹) once again became the dominating profile. It should be noted that the middle peak that appeared in Fig. 8c after warming to 150 K and cooling back down is most likely due to an interaction of CO₂ and H₂O and may not be solely attributed to CO₂ (Bernstein et al., 2005). The 2.697 μm (3708 cm⁻¹) peak remained the dominating absorption profile while cooling until at 85 K the peak at 2.707 μm (3694 cm⁻¹) became about 10% stronger, though about twice as broad as the 2.697 μm (3708 cm⁻¹) absorption profile.

The $2\nu_2 + \nu_3$ mode appeared at the deposition temperature around 2.786 μm (3590 cm⁻¹) as a small, broad peak (\leq 10% the

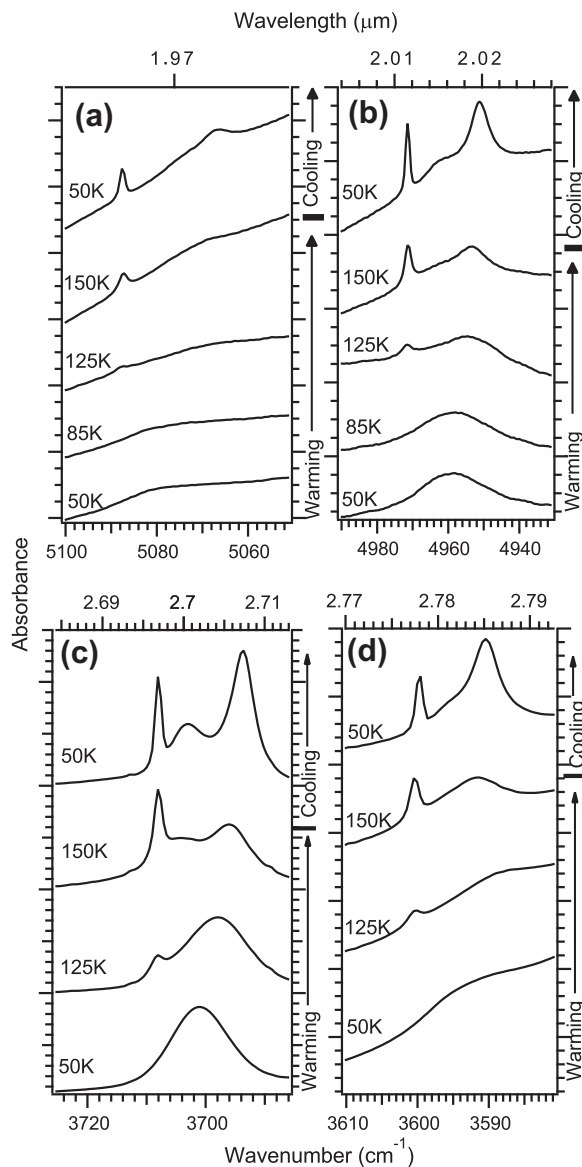


Fig. 8. (a) CO₂ $2\nu_1 + \nu_3$, (b) $\nu_1 + 2\nu_2 + \nu_3$, (c) CO₂ $\nu_1 + \nu_3$, and (d) $2\nu_2 + \nu_3$ profiles in a mixture of H₂O + CH₃OH + CO₂ (10:1:1) deposited at 50 K and heated at a rate of 2 K min⁻¹ to 150 K and cooled down. Spectra were taken as the sample was held at the indicated temperature.

intensity of the $\nu_1 + \nu_3$ feature) on the side of the O–H stretching mode of H₂O and CH₃OH near 2.954 μm (3385 cm⁻¹) making this absorption profile difficult to analyze (Fig. 8d). A second peak appeared around 2.778 μm (3600 cm⁻¹) at 120 K with about the same height as the 2.786 μm (3590 cm⁻¹) feature. This peak became sharper as the sample was heated to 150 K. The two peaks became more distinct after cooling back down to 50 K.

3.2.2. CH₃OH-rich mixtures

Experiments with more than 50% CH₃OH (both binary and ternary mixtures) yielded absorption profiles similar to those of H₂O-dominated mixtures, due to some modes being on the large O–H stretch mode of CH₃OH and/or H₂O and the absorption curve between 1.67 and 2.5 μm (e.g., Fig. 2). As a representation of CH₃OH-dominated ice mixtures, Fig. 9 contains selected spectra of a H₂O + CH₃OH + CO₂ (1:10:1) ice deposited at 15 K, heated at a rate of 2 K min⁻¹ to 120 K and cooled down.

The barely visible $2\nu_1 + \nu_3$ mode near 1.974 μm (5066 cm⁻¹) became broader and weaker (height about 5% or less than that of

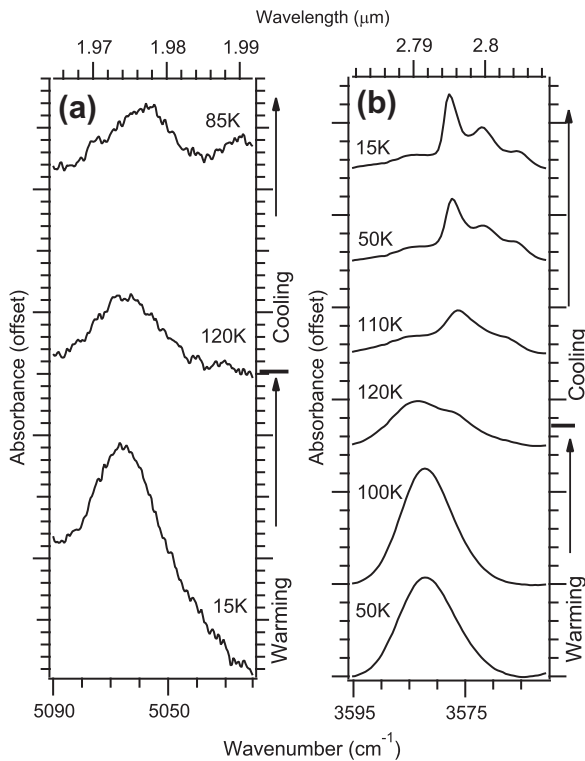


Fig. 9. Spectra from a mixture of $\text{H}_2\text{O} + \text{CH}_3\text{OH} + \text{CO}_2$ (1:10:1) deposited at 50 K and heated at a rate of 2 K min^{-1} to 120 K and cooled down. Spectra were taken as the sample was held at the indicated temperature. The CO_2 mode profiles of (a) $2\nu_1 + \nu_3$ and (b) $2\nu_2 + \nu_3$ are shown. The noisiness in (a) is due to the weakening of the feature.

the stronger $\nu_1 + \nu_3$ feature), shifting to a higher wavelength when warming up from 15 K (Fig. 9a). This feature continued to weaken and shift by as much as $0.01 \mu\text{m}$ (8 cm^{-1}), even when cooling down and disappeared completely when the sample cooled to 75 K.

The $\nu_1 + \nu_3$ mode appeared near $2.712 \mu\text{m}$ (3695 cm^{-1}) and remained the strongest CO_2 feature in this spectral range throughout the heating/cooling process, as it did in the H_2O -dominated mixtures. The position did not change when heating to 120 K. Upon cooling, however, the peak shifted to $2.711 \mu\text{m}$ (3690 cm^{-1}) at 110 K and gradually to $2.710 \mu\text{m}$ (3689 cm^{-1}) when cooling to 15 K.

The $2\nu_2 + \nu_3$ mode near $2.792 \mu\text{m}$ (3582 cm^{-1}) appeared as a stronger feature (about half the height of the $\nu_1 + \nu_3$ mode) in CH_3OH -dominated mixtures compared to the same feature in H_2O -dominated mixtures, though it was still difficult to analyze due to its proximity to the large O–H stretch mode. This absorption profile began to split into three peaks as the sample was cooled from 120 K to 15 K (Fig. 9b) with the dominate feature near $2.795 \mu\text{m}$ (3578 cm^{-1}) and the other two peaks at $2.800 \mu\text{m}$ (3572 cm^{-1}) and $2.804 \mu\text{m}$ (3566 cm^{-1}) (about half and one-fourth the height of the dominate peak, respectively). This splitting and increase of intensity of the $2.795 \mu\text{m}$ feature is likely due to the interaction of $\text{H}_2\text{O} - \text{CH}_3\text{OH}$ complexes trapping CO_2 molecules in separate pockets of ice (Section 1).

3.3. High-temperature deposits

Observations of the IR absorption features of H_2O in the outer Solar System revealed that most ices exist in a crystalline phase instead of an amorphous structure. Specifically, crystalline phases of H_2O -ice such as I_c (cubic phase) and I_h (hexagonal phase) are the dominate forms of H_2O in the Solar System (e.g., Cruikshank

et al., 1998; Schmitt et al., 1998). However, this does not necessarily mean that the absorption profiles of the ice indicate that the temperatures of the ices on planetary surfaces are currently at or above the phase transition temperature of the H_2O -ice component. Rather, it is possible that the ice had been heated to those temperatures at some point in the past and cooled back down (e.g., Ehrenfreund et al., 1999; White et al., 2009). This raises the question as to whether CO_2 seen in these ices is a trapped remnant of an earlier, lower temperature interval or whether it can be directly deposited at or above the crystalline phase transition temperatures of solid H_2O . Previous experiments have demonstrated that the trapping efficiency and residence time of CO_2 in H_2O drops rapidly at temperatures above 90 K and little or no CO_2 is trapped above 100 K at deposition rates of about $0.09 \mu\text{m min}^{-1}$ (Sandford and Allamandola, 1990b; Gálvez et al., 2008). It is possible that CO_2 could be trapped in H_2O -rich ices at higher temperatures if deposition rates are higher. At higher temperatures, the residence time of a CO_2 molecule on an H_2O -ice surface are decreased, but the CO_2 could still be trapped if the next overlying layer of H_2O is deposited quickly enough (Sandford and Allamandola, 1990b). We varied the deposition rates of some H_2O , CH_3OH , and CO_2 mixtures in this paper to explore the extent to which CO_2 can be deposited in H_2O -ices above 100 K.

Experiments were performed with mixtures of $\text{H}_2\text{O} + \text{CO}_2$ (20:1), $\text{H}_2\text{O} + \text{CH}_3\text{OH} + \text{CO}_2$ (10:1:1), $\text{H}_2\text{O} + \text{CH}_3\text{OH} + \text{CO}_2$ (100:10:1), and $\text{H}_2\text{O} + \text{CH}_3\text{OH} + \text{CO}_2$ (1:10:1) with three different deposition rates; a “fast” rate of $\sim 0.5 \mu\text{m min}^{-1}$, a “slow” rate of $\leq 0.03 \mu\text{m min}^{-1}$, and an “intermediate” rate that corresponds to our normal rate of $\sim 0.1 \mu\text{m min}^{-1}$. These studies were performed to verify the earlier observations of Sandford and Allamandola (1990a) and to see whether or not CO_2 could be trapped in H_2O ices at higher temperatures with higher deposition rates. Thicknesses were similar to previous high-temperature deposit experiments (~ 0.3 – $1.0 \mu\text{m}$). Table 2 contains the highest deposition temperatures at which CO_2 was detected in the resulting ice mixtures at the three different deposition rates.

The CO_2 asymmetric stretch mode was just visible as a small peak when a sample of $\text{H}_2\text{O} + \text{CO}_2$ (20:1) was deposited at 110 K at a rate of about $0.1 \mu\text{m min}^{-1}$, indicating a trace amount of resident CO_2 ($<1\%$ relative to H_2O , Fig. 10). All of the CO_2 asymmetric stretch mode profiles in successful deposits of CO_2 above 100 K resembled this experiment. Note the deformation of the O–H stretch mode in Fig. 10 that suggests a crystalline phase of H_2O . CO_2 could be trapped at higher temperatures if higher deposition rates are used, although the differences are not dramatic. At the fastest deposition rate of $0.5 \mu\text{m min}^{-1}$ CO_2 could be partially trapped at temperatures as high as 120 K for $\text{H}_2\text{O}:\text{CO}_2$ ratios of 10:1 or 20:1. However, faster deposits of $\text{H}_2\text{O} + \text{CH}_3\text{OH} + \text{CO}_2$

Table 2

Highest temperatures at which CO_2 was present when H_2O , CH_3OH , and CO_2 mixtures were deposited at temperatures above 50 K. CO_2 was determined to have deposited out if the ν_3 asymmetric stretch mode was visible in the mid-IR spectrum.

Mixture	Temperature (K)	Deposition rate ($\mu\text{m min}^{-1}$)
$\text{H}_2\text{O} + \text{CO}_2$ (20:1)	110	≤ 0.03 and 0.1
	120	~ 0.5
$\text{CH}_3\text{OH} + \text{CO}_2$ (5:1)	100	≤ 0.03 and 0.1
	115	~ 0.5
$\text{H}_2\text{O} + \text{CH}_3\text{OH} + \text{CO}_2$ (10:1:1)	115	≤ 0.03 and 0.1
	120	~ 0.5
	115	~ 0.5
	110	≤ 0.03 and 0.1
(100:10:1)	115	~ 0.5
	115	~ 0.5
(1:10:1)	110	≤ 0.03 and 0.1
	115	~ 0.5
(10:10:1)	110	≤ 0.03 and 0.1

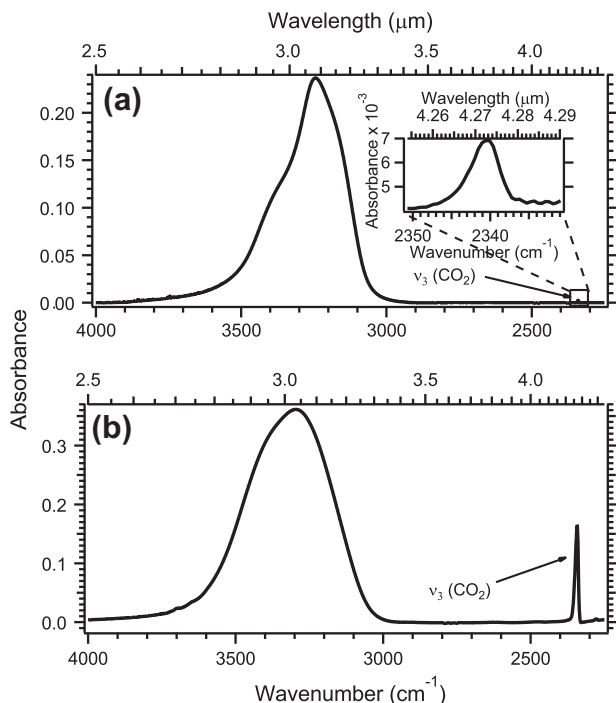


Fig. 10. Spectrum from a mixture of (a) H₂O + CO₂ (20:1) deposited at 110 K at a rate of $\sim 0.1 \mu\text{m min}^{-1}$ to a thickness of about $0.2 \mu\text{m}$ compared with (b) a spectrum from H₂O + CO₂ (24:1) deposited at 15 K at a rate of $\sim 0.1 \mu\text{m min}^{-1}$ to a thickness of about $0.3 \mu\text{m}$.

(100:10:1 and 100:50:1) yielded CO₂ at temperatures no greater than 115 K (Table 2).

Some CO₂ was visible in the CH₃OH-rich spectra at the same temperatures as observed in the H₂O-dominated mixtures (e.g., 100 K, 110 K). Faster deposits ($0.5 \mu\text{m min}^{-1}$) of H₂O + CH₃OH + CO₂ (1:10:1) yielded CO₂ at temperatures no greater than 115 K, similar to the H₂O-rich experiments above. In H₂O + CH₃OH + CO₂ (10:10:1) experiments, CO₂ was not visible when depositing above 100 K. No double peaks on the CO₂ stretch mode were visible when depositing at 65 K and above. Evidently, the more CH₃OH present, the less likely CO₂ will reside in an ice deposited above 100 K.

The ν_3 CO₂ asymmetric stretch mode was clearly visible at deposition temperatures up to 100 K when samples were deposited at a rate of $\leq 0.1 \mu\text{m min}^{-1}$. The position of the CO₂ asymmetric stretch mode at deposition also coincided with the same position as a mixture deposited at 15 or 50 K and warmed up to that temperature. For example, depositing a H₂O-rich sample at 85 K yielded a ν_3 asymmetric stretch mode at $4.272 \mu\text{m}$ (2341 cm^{-1}) – the same position observed when warming to 85 K from a deposition at 50 K. The results of these studies support earlier findings (e.g., Sandford and Allamandola, 1990b; Gálvez et al., 2008) who saw little or no CO₂ trapping when samples were deposited above 100 K. However, the results here show that some CO₂ can be trapped at temperatures up to 120 K when faster deposits ($\sim 0.5 \mu\text{m min}^{-1}$) are used. The findings in this study suggest that it is possible for CO₂ to deposit out and reside in higher temperature H₂O-dominated ice mixtures if deposition rates are elevated. However, the amount of resident CO₂ decreases exponentially with temperature (note the differences in the ν_3 CO₂ asymmetric stretch mode in Fig. 10).

4. Discussion

The position(s) of the ν_3 CO₂ asymmetric stretch mode feature shifted to a longer wavelength (smaller wavenumber) as the

sample was heated in both H₂O- and CH₃OH-rich ices (Fig. 3) in response to molecular migration (Section 1). Shifting of the absorption bands observed in these experiments with all ice mixtures, both H₂O- and CH₃OH-rich, indicate a restructuring of the ice matrix as the samples are heated. Unlike most mixtures, the position of the CO₂ ν_3 asymmetric stretch mode seems to migrate back and forth when heating and cooling between 70 and 120 K in the H₂O + CO₂ (24:1) mixture. This is perhaps due to the low to high density amorphous phase changes happening in this range (Blake et al., 1991). Though the mixture H₂O + CH₃OH + CO₂ (10:1:1) was often used as a typical example, mixtures with H₂O:CO₂ ratios of 100:1 yielded spectra with fewer visible combination and overtone modes of CO₂ ($1.25\text{--}2.04 \mu\text{m}$ or $8000\text{--}4900 \text{ cm}^{-1}$, – see also Table 1). It should be noted that saturation of the bands makes it difficult to determine position and other properties such as column density of the species (the asymmetric CO₂ stretch mode, for example). This was only an issue if ice thicknesses exceeded $2 \mu\text{m}$ for the mid-IR experiments and the concentration of H₂O:CO₂ was 2:1 or so (Section 2.3).

Sometimes this feature split into multiple peaks, particularly in binary mixtures of H₂O + CO₂ and CH₃OH + CO₂. This is most likely due to molecular rearrangement, segregation, and phase changes in the ice (Sandford and Allamandola, 1990a; Öberg et al., 2009). Peak splitting is also affected by how much H₂O is present and the thickness of the sample. Also, some of the double-peaked absorption profiles of the ν_3 CO₂ asymmetric stretch mode may suggest the formation of clathrate hydrates (type I) (Blake et al., 1991; Dartois and Schmitt, 2009). The splitting and increase of intensity of the $2\nu_2 + \nu_3$ CO₂ mode is likely due to the interaction of H₂O – CH₃OH complexes trapping CO₂ molecules in separate pockets of ice (Section 3.2.2, Blake et al. (1991); Tielens (2005)). The presence of CH₃OH appears to strongly influence many absorption features of CO₂, as has been demonstrated in previous studies (e.g., Sandford and Allamandola, 1993; Marchand et al., 2006; Maté et al., 2009; White et al., 2009; White, 2010). The influence of CH₃OH on the absorption profiles is strong due to the possibility of stronger bonds between CH₃OH and H₂O, thus forming more complex structures trapping CO₂ molecules (Collings et al., 2004). Also, the carbon atom of CO₂ can act as a Lewis acid because part of the electron density is removed due to the existence of two electronegative O atoms (Kazarian et al., 1996; Klotz et al., 2004). The presence of CH₃OH may also affect the sticking efficiency of CO₂ in ice mixtures deposited at higher temperatures ($>50 \text{ K}$) as suggested in Section 5.

5. Comparison to astronomical data

The position of the vibrational mode of CO₂ in astronomical observations is consistent with laboratory spectra of a H₂O-dominated ice sample containing CO₂ as seen in this study, and, for example, experiments by Sandford and Allamandola (1990a), Cruikshank et al. (2010), and in theoretical models from Chaban et al. (2007). The addition of CH₃OH also induces a slight shift ($\leq 0.01 \mu\text{m}$ or 1 cm^{-1}) but mainly changes the appearance of the absorption profiles (e.g., Ehrenfreund et al., 1998; White et al., 2009; Cruikshank et al., 2010).

Some examples of observed temperatures and spectral positions of the CO₂ stretch mode from some jovian and saturnian satellites along with the ranges of temperatures and positions of this feature in laboratory data from this study are shown in Fig. 11. Observations were taken from published data from ground-based telescopes, NIMS aboard the Galileo spacecraft, and VIMS aboard the Cassini probe (Grundy et al., 1999; Hibbitts et al., 2000, 2003; Ostro et al., 2006; Cruikshank et al., 2007, 2010). Temperatures for the surfaces of the jovian satellites, Dione, and Iapetus were derived from an average disk temperature and the IR

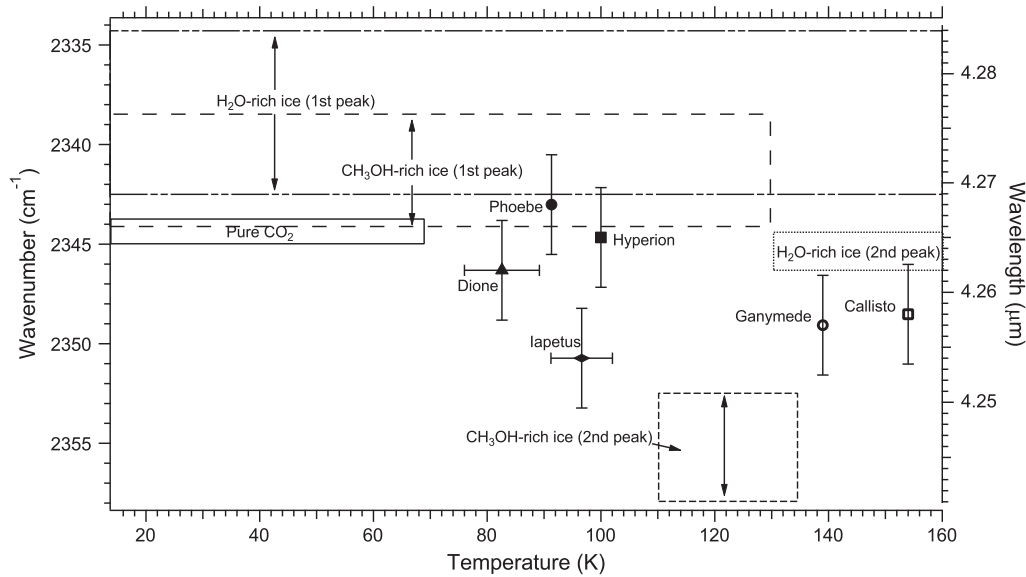


Fig. 11. Observed temperatures of some jovian and saturnian satellites and positions of the CO₂ stretch mode in IR absorption spectra compared with positions and temperatures of CO₂ stretch mode profiles in laboratory data from this study. Asymmetric stretch mode band positions are from the following: the saturnian satellite surfaces are from Cruikshank et al. (2010), the surface of Ganymede is from Hibbitts et al. (2003), and the surface of Callisto is from Hibbitts et al. (2000). Surface temperatures of Dione, Iapetus, and the jovian satellites are from Grundy et al. (1999), of Phoebe is from Ostro et al. (2006), and of Hyperion is from Cruikshank et al. (2007). The ranges with which the CO₂ stretch mode feature migrates in the laboratory are marked with boxes. “2nd Peak” refers to the second feature that appears at temperatures greater than 110 K in some of the H₂O- and CH₃OH-rich mixtures in addition to the primary feature, or “1st Peak”.

absorption features of H₂O-ice from the surfaces (Grundy et al., 1999). Temperatures for Phoebe and Hyperion were derived from observed albedo and average disk temperature (Ostro et al., 2006; Cruikshank et al., 2007). “2nd Peak” in the figure refers to the second feature that appears at temperatures greater than 110 K in some of the H₂O- and CH₃OH-rich mixtures in addition to the primary feature, or “1st Peak”.

In H₂O- and CH₃OH-rich ices, a second peak would often appear in the ν_3 asymmetric stretch mode of CO₂ at a shorter wavelength (larger wavenumber) and is labeled as e.g., “H₂O-rich ice 2nd Peak” in addition to the primary peak or “1st Peak” (e.g., Section 3.1.1). From Fig. 11, it is obvious that pure CO₂ is not likely a component on the surfaces of these satellites. It is also unlikely that CH₃OH-rich ices are components and none of the data match up to “Peak 2” of the CH₃OH-rich laboratory data. However, the CO₂ asymmetric stretch mode appears near $\sim 4.255 \mu\text{m}$ ($\sim 2350 \text{ cm}^{-1}$) for the Ganymede and Callisto surfaces getting close to the Peak 2 of H₂O-rich laboratory ices. It is evident that the surfaces of Phoebe, Dione, and Hyperion likely contain ices dominated by H₂O and perhaps CH₃OH. It should also be noted, however, that though many of the observational data do not confirm the presence of CH₃OH, the laboratory data in this study offer a means of exploring that possibility. Experiments in this study have demonstrated that in CO₂ ices with more than H₂O present (CH₃OH, in this case) the position of the CO₂ ν_3 asymmetric stretch mode changes very little when the sample is cooled from 140 K after heating. This may suggest that the ice on many of the outer planetary surfaces are at (or once were at) temperatures near or above the glass transition temperature of H₂O (130–140 K).

These data and the data from this paper demonstrate that the spectral characteristics of an ice are dominated by the highest temperature to which the ice has been. However, CO₂ ν_3 asymmetric stretch band positions do not match laboratory band positions for Dione, Iapetus, or Ganymede at all. This means there are more species present in the ice affecting the CO₂ band positions, there is or have been UV processing of the icy surfaces of these satellites, or a combination of both. Though the laboratory data in this study begin to explain the chemistry of these satellites’ surfaces, many

more parameters need to be explored in the laboratory to get a more complete picture.

6. Conclusions

These data explore parameters and permutations of astrophysically relevant ice mixtures in the laboratory. Absorption spectra from solid CO₂ are sensitive indicators of temperature and composition. Position of the absorption features of CO₂ were different at deposition depending on the ratios of H₂O and CH₃OH. The ν_3 asymmetric stretch mode of CO₂ yielded different results, depending on the ratio of H₂O and CH₃OH. Mixtures where H₂O was the dominant species yielded similar results, as did CH₃OH-dominated mixtures. Interestingly, the H₂O + CO₂ (24:1) mixture seemed to allow the ν_3 asymmetric stretch mode to move back and forth when heating and cooling between ~ 70 and 120 K. CH₃OH-rich mixtures thermally processed yielded similar results in the amount the CO₂ asymmetric stretch mode shifted, though the positions were different. When combined with H₂O, however, CH₃OH seems to have a strong influence on position of the ν_3 asymmetric stretch mode as it seems result in shifting during the heating and cooling process, likely due the strong contribution of CH₃OH in the clathrate forming process (e.g., Fig. 3 and Section 1).

The near-IR vibrational modes of CO₂ were more difficult to analyze, as expected, due to the much lower relative intensity and widths of the absorption peaks compared to the strong absorption features of H₂O and CH₃OH. Some of the extra peaks that appear such as the “broad feature” in Fig. 8a, the middle peak in Fig. 8c, and the multi-peak features in Fig. 9b are most likely due to an interaction of H₂O and CO₂, as discussed earlier (Bernstein et al., 2005). Still, a distinct correlation between temperature and mixture ratios were noted in all binary and ternary H₂O, CH₃OH, and CO₂ mixtures.

In the high-temperature deposition experiments, we concluded that it is possible to deposit CO₂ in H₂O-dominated ice mixtures at temperatures up to 120 K. This is only possible, however, if the deposition rate is $0.5 \mu\text{m min}^{-1}$ or at least greater than $0.1 \mu\text{m min}^{-1}$ (Table 2). This pushes the previously calculated

highest temperature that CO₂ will deposit out in an ice (Sandford and Allamandola, 1990b) by 10 K higher to 120 K. Though only appearing in trace amounts ($\leq 1\%$), the ν_3 asymmetric stretch mode of CO₂ appears at the same position as it would had the mixture been deposited at a low temperature (≤ 50 K) and warmed up at a rate of 2 K min⁻¹ to the deposition temperature. Clearly the IR absorption spectrum reflects the highest temperature to which the ice has been in the past. However, the ice may have deposited at a higher temperature in the first place. These results may provide another variable and perspective on ice formation, particularly in the Solar System.² This may help to explain some of the ν_3 asymmetric stretch mode positions from the surfaces of the jovian and saturnian satellites as they vary from the laboratory experiments in this study where the ice was deposited at ≤ 50 K (Fig. 11), though there are many other parameters to explore in the laboratory (UV photolysis, H₂O-rich ices with molecules other than CH₃OH and CO₂, etc.).

Acknowledgments

The authors thank NASA and Oak Ridge Associated Universities for sponsoring the NASA Postdoctoral Program (NPP) and NASA's Origins of Solar Systems and Planetary Geology and Geophysics Programs for support. We also thank Perry Gerakines and the University of Alabama at Birmingham (UAB) for use of some of the data in this study.

References

- Allamandola, L.J., Sandford, S.A., Tielens, A.G.G.M., Herbst, T.M., 1992. Infrared spectroscopy of dense clouds in the C–H stretch region-methanol and 'diamonds'. *Astrophys. J.* 399 (November), 134–146.
- Angell, C.A., 2002. Liquid fragility and the glass transition in water and aqueous solutions. *Chem. Rev.* 102 (8), 2627–2650.
- Baragiola, R.A., 2003. Water in Confining Geometries: Properties of Microporous ASW Thin Films. Springer-Verlag, Berlin, Heidelberg, pp. 359–395.
- Bernstein, M.P., Sandford, S.A., Allamandola, L.J., Chang, S., Scharberg, M.A., 1995. Organic compounds produced by photolysis of realistic interstellar and cometary ice analogs containing methanol. *Astrophys. J.* 454 (November), 327–344.
- Bernstein, M.P., Cruikshank, D.P., Sandford, S.A., 2005. Near-infrared laboratory spectra of solid H₂O/CO₂ and CH₃OH/CO₂ ice mixtures. *Icarus* 179 (December), 527–534.
- Bernstein, M.P., Cruikshank, D.P., Sandford, S.A., 2006. Near-infrared spectra of laboratory H₂O–CH₄ ice mixtures. *Icarus* 181 (March), 302–308.
- Blake, D., Allamandola, L., Sandford, S., Hudgins, D., Freund, F., 1991. Clathrate hydrate formation in amorphous cometary ice analogs in vacuo. *Science* 245, 548–551.
- Carlson, R. et al., 1996. Near-infrared spectroscopy and spectral mapping of Jupiter and the Galilean satellites: Results from Galileo's initial orbit. *Science* 274 (October), 385–388.
- Chaban, G.M., Bernstein, M., Cruikshank, D.P., 2007. Carbon dioxide on planetary bodies: Theoretical and experimental studies of molecular complexes. *Icarus* 187 (April), 592–599.
- Chiar, J.E., Adamson, A.J., Kerr, T.H., Whittet, D.C.B., 1995. High-resolution studies of solid CO in the taurid dark cloud: Characterizing the ices in quiescent clouds. *Astrophys. J.* 455 (December), 234–243.
- Collings, M.P. et al., 2004. A laboratory survey of the thermal desorption of astrophysically relevant molecules. *Mem. R. Astron. Soc.* 354 (November), 1133–1140.
- Cruikshank, D.P. et al., 2007. Surface composition of Hyperion. *Nature* 448 (July), 54–56.
- Cook, A.M., Whittet, D.C.B., Shenoy, S.S., Gerakines, P.A., White, D.W., Chiar, J.E., 2011. The thermal evolution of ices in the environments of newly formed stars: The CO₂ diagnostic. *Astrophys. J.* 730 (April), 124–139.
- Cruikshank, D.P., Brown, R.H., Calvin, W.M., Roush, T.L., Bartholomew, M.J., 1998. Ices on the satellites of Jupiter, Saturn, and Uranus. In: Schmitt, B., de Bergh, C., Festou, M. (Eds.), *Solar System Ices. Astrophysics and Space Science Library*, vol. 227. p. 579.
- Cruikshank, D.P., Meyer, A.W., Brown, R.H., Clark, R.N., Jaumann, R., Stephan, K., Hibbitts, C.A., Sandford, S.A., Mastrapa, R.M.E., Filacchione, G., Ore, C.M.D., Nicholson, P.D., Buratti, B.J., McCord, T.B., Nelson, R.M., Dalton, J.B., Baines, K.H., Matson, D.L., 2010. Carbon dioxide on the satellites of Saturn: Results from the Cassini VIMS investigation and revisions to the VIMS wavelength scale. *Icarus* 206 (April), 561–572.
- Cyriac, J., Pradeep, T., 2008. Structural reorganization on amorphous ice films below 120 K revealed by near-thermal (~ 1 eV) ion scattering. *J. Phys. Chem. C* 112 (13), 5129–5135.
- Dartois, E., Schmitt, B., 2009. Carbon dioxide clathrate hydrate FTIR spectrum. Near infrared combination modes for astrophysical remote detection. *Astron. Astrophys.* 504 (September), 869–873.
- Dartois, E., Demyk, K., d'Hendecourt, L., Ehrenfreund, P., 1999. Carbon dioxide-methanol intermolecular complexes in interstellar grain mantles. *Astron. Astrophys.* 351 (November), 1066–1074.
- Dohnálek, Z., Kimmel, G.A., Ayotte, P., Smith, R.S., Kay, B.D., 2003. The deposition angle-dependent density of amorphous solid water films. *J. Chem. Phys.* 118 (January), 364–372.
- Ehrenfreund, P., 1990. An ISO view on interstellar and cometary ice chemistry. *Space Sci. Rev.* 50 (October), 233–238.
- Ehrenfreund, P. et al., 1996. A laboratory database of solid CO and CO₂ for ISO. *Astron. Astrophys.* 315 (November), L341–L344.
- Ehrenfreund, P. et al., 1999. Laboratory studies of thermally processed H₂O–CH₃OH–CO₂ ice mixtures and their astrophysical implications. *Astron. Astrophys.* 350 (October), 240–253.
- Ehrenfreund, P., Boogert, A.C.A., Gerakines, P.A., Tielens, A.G.G.M., van Dishoeck, E.F., 1997. Infrared spectroscopy of interstellar apolar ice analogs. *Astron. Astrophys.* 328 (December), 649–669.
- Ehrenfreund, P., Dartois, E., Demyk, K., D'Hendecourt, L., 1998. Ice segregation toward massive protostars. *Astron. Astrophys.* 339 (November), L17–L20.
- Fink, U., Larson, H.P., Gautier Jr., T.N., Treffers, R.R., 1976. Infrared spectra of the satellites of Saturn – Identification of water ice on Iapetus, Rhea, Dione, and Tethys. *Astrophys. J.* 207 (July), L63–L67.
- Fleyfel, F., Devlin, J.P., 1991. Carbon dioxide clathrate hydrate epitaxial growth: Spectroscopic evidence for formation of the simple type-II CO₂ hydrate. *J. Phys. Conf. Ser.* 95, 3811–3815.
- Gálvez, O. et al., 2007. A study of the interaction of CO₂ with water ice. *Astron. Astrophys.* 472 (September), 691–698.
- Gálvez, Ó., Maté, B., Herrero, V.J., Escribano, R., 2008. Trapping and adsorption of CO₂ in amorphous ice: A FTIR study. *Icarus* 197 (October), 599–605.
- Gerakines, P.A. et al., 1999. Observations of solid carbon dioxide in molecular clouds with the infrared space observatory. *Astrophys. J.* 522 (September), 357–377.
- Gerakines, P.A., Bray, J.J., Davis, A., Richey, C.R., 2005. The strengths of near-infrared absorption features relevant to interstellar and planetary ices. *Astrophys. J.* 620 (February), 1140–1150.
- Gibb, E.L. et al., 2000. An inventory of interstellar ices toward the embedded protostar W33A. *Astrophys. J.* 536 (June), 347–356.
- Grundy, W.M., Buie, M.W., Stansberry, J.A., Spencer, J.R., Schmitt, B., 1999. Near-infrared spectra of icy outer Solar System surfaces: Remote determination of H₂O ice temperatures. *Icarus* 142 (December), 536–549.
- Grundy, W.M., Young, L.A., Spencer, J.R., Johnson, R.E., Young, E.F., Buie, M.W., 2006. Distributions of H₂O and CO₂ ices on Ariel, Umbriel, Titania, and Oberon from IRTF/SpEx observations. *Icarus* 184 (October), 543–555.
- Hale, G.M., Querry, M.R., 1973. Optical constants of water in the 200-nm to 200- μ m wavelength region. *Appl. Opt.* 12 (March), 555–563.
- Herbst, E., 2001. The chemistry of interstellar space. *Chem. Soc. Rev.* 30, 168–176.
- Hibbitts, C.A., McCord, T.B., Hansen, G.B., 2000. Distributions of CO₂ and SO₂ on the surface of Callisto. *J. Geophys. Res.* 105 (September), 22541–22558.
- Hibbitts, C.A., Klemaszewski, J.E., McCord, T.B., Hansen, G.B., Greeley, R., 2002. CO₂-rich impact craters on Callisto. *J. Geophys. Res. (Planets)* 107 (October), 5084–5096.
- Hibbitts, C.A., Pappalardo, R.T., Hansen, G.B., McCord, T.B., 2003. Carbon dioxide on Ganymede. *J. Geophys. Res. (Planets)* 108 (May), 5036–5058.
- Hodyss, R., Johnson, P.V., Orzechowska, G.E., Goguen, J.D., Kanik, I., 2008. Carbon dioxide segregation in 1:4 and 1:9 CO₂:H₂O ices. *Icarus* 194 (April), 836–842.
- Hornekaer, L., Baurichter, A., Petrunin, V.V., Luntz, A.C., Kay, B.D., Al-Halabi, A., 2005. Influence of surface morphology on d₂ desorption kinetics from amorphous solid water. *J. Chem. Phys.* 122 (12), 124701–124712.
- Hudgins, D.M., Sandford, S.A., Allamandola, L.J., Tielens, A.G.G.M., 1993. Mid- and far-infrared spectroscopy of ices – Optical constants and integrated absorbances. *Astrophys. J. Suppl. Ser.* 86 (June), 713–870.
- Hudson, R.L., Moore, M.H., 2000. Note: IR spectra of irradiated cometary ice analogues containing methanol: A new assignment, a reassignment, and a nonassignment. *Icarus* 145 (June), 661–663.
- Hudson, R.L., Moore, M.H., 2001. Radiation chemical alterations in Solar System ices: An overview. *J. Geophys. Res.* 106 (December), 33275–33284.
- Jenniskens, P., Blake, D.F., 1996. Crystallization of amorphous water ice in the Solar System. *Astrophys. J.* 473 (December), 1104–1113.
- Jenniskens, P., Blake, D.F., Wilson, M.A., Pohorille, A., 1995. High-density amorphous ice, the frost on interstellar grains. *Astrophys. J.* 455 (January), 389–401.
- Kazarian, S.G., Vincent, M.F., Bright, F.V., Liotta, C.L., Eckert, C.A., 1996. Specific intermolecular interaction of carbon dioxide with polymers. *J. Am. Chem. Soc.* 118 (7), 1729–1736.
- Klotz, A., Ward, T., Dartois, E., 2004. Molecular complexes theoretical computations between methanol and carbon dioxide and their implications in the interstellar ice mantles. *Astron. Astrophys.* 416 (March), 801–810.
- Kohl, I., Mayer, E., Hallbrucker, A., 2000. The glassy water cubic ice system: A comparative study by X-ray diffraction and differential scanning calorimetry. *Phys. Chem. Chem. Phys. (Incorporat. Faraday Trans.)* 2, 1579–1586.
- Lacy, J.H., Faraji, H., Sandford, S.A., Allamandola, L.J., 1998. Unraveling the 10 μ m "silicate" feature of protostars: The detection of frozen interstellar ammonia. *Astrophys. J.* 501 (1), L105–L109.

² e.g., <http://www.astrochemistry.org/db.php>.

- Marchand, P., Riou, R., Ayote, P., 2006. Diffusion kinetics for methanol in polycrystalline ice. *J. Phys. Chem. A* 110 (September), 11654–11664.
- Mastrapa, R.M., Bernstein, M.P., Sandford, S.A., Roush, T.L., Cruikshank, D.P., Ore, C.M.D., 2008. Optical constants of amorphous and crystalline H₂O-ice in the near infrared from 1.1 to 2.6 μm . *Icarus* 197 (September), 307–320.
- Maté, B., Gálvez, Ó., Herrero, V.J., Escribano, R., 2009. Infrared spectra and thermodynamic properties of CO₂/methanol ices. *Astrophys. J.* 690 (January), 486–495.
- McCord, T.B. et al., 1998. Salts on Europa's surface detected by Galileo's near infrared mapping spectrometer. *Science* 280 (May), 1242–1245.
- Moore, M.H., Hudson, R.L., Gerakines, P.A., 2001. Mid- and far-infrared spectroscopic studies of the influence of temperature ultraviolet photolysis and ion irradiation on cosmic-type ices. *Spectrochim. Acta* 57 (March), 843–858.
- Öberg, K.I. et al., 2007. Effects of CO₂ on H₂O band profiles and band strengths in mixed H₂O:CO₂ ices. *Astron. Astrophys.* 462 (February), 1187–1198.
- Öberg, K.I., Fayolle, E.C., Cuppen, H.M., van Dishoeck, E.F., Linnartz, H., 2009. Quantification of segregation dynamics in ice mixtures. *Astron. Astrophys.* 505 (October), 183–194.
- Ostro, S.J., West, R.D., Janssen, M.A., Lorenz, R.D., Zebker, H.A., Black, G.J., Lunine, J.I., Wye, L.C., Lopes, R.M., Wall, S.D., Elachi, C., Roth, L., Hensley, S., Kelleher, K., Hamilton, G.A., Gim, Y., Anderson, Y.Z., Boehmer, R.A., Johnson, W.T.K. the Cassini RADAR Team, 2006. Cassini RADAR observations of Enceladus, Tethys, Dione, Rhea, Iapetus, Hyperion, and Phoebe. *Icarus* 183 (August), 479–490.
- Quirico, E., Schmitt, B., 1997. Near-infrared spectroscopy of simple hydrocarbons and carbon oxides diluted in solid N₂ and as pure ices: Implications for Triton and Pluto. *Icarus* 127 (June), 354–378.
- Salama, F., Allamandola, L.J., Sandford, S.A., Bregman, J.D., Witteborn, F.C., Cruikshank, D.P., 1994. Is H₂O present on Io? The detection of a new strong band near 3590 cm⁻¹ (2.79 μm). *Icarus* 107 (February), 413–417.
- Sandford, S.A., Allamandola, L.J., 1990a. The physical and infrared spectral properties of CO₂ in astrophysical ice analogs. *Astrophys. J.* 355 (May), 357–372.
- Sandford, S.A., Allamandola, L.J., 1990b. The volume- and surface-binding energies of ice systems containing CO, CO₂, and H₂O. *Icarus* 87 (September), 188–192.
- Sandford, S.A., Allamandola, L.J., 1993. Condensation and vaporization studies of CH₃OH and NH₃ ices: Major implications for astrochemistry. *Astrophys. J.* 417 (November), 815–825.
- Sandford, S.A., Bernstein, M.P., Allamandola, L.J., Goorvitch, D., Teixeira, T.C.V.S., 2001. The abundances of solid N₂ and gaseous CO₂ in interstellar dense molecular clouds. *Astrophys. J.* 548 (February), 836–851.
- Schmitt, B., Quirico, E., Trotta, F., Grundy, W.M., 1998. Optical properties of ices from UV to infrared. In: Schmitt, B., de Bergh, C., Festou, M. (Eds.), *Solar System Ices. Astrophysics and Space Science Library*, vol. 227. p. 199.
- Smith, R., 2000. The self-diffusivity of amorphous solid water near 150 K. *Chem. Phys.* 258 (August), 291–305.
- Tielens, A.G.G.M., 2005. The physics and chemistry of the interstellar medium. In: Tielens, A.G.G.M. (Ed.), *The Physics and Chemistry of the Interstellar Medium*. Cambridge University Press, Cambridge, UK, ISBN:0521826349.
- Tielens, A.G.G.M., Hagen, W., 1982. Model calculations of the molecular composition of interstellar grain mantles. *Astron. Astrophys.* 114 (October), 245–260.
- van Broekhuizen, F.A., Groot, I.M.N., Fraser, H.J., van Dishoeck, E.F., Schlemmer, S., 2006. Infrared spectroscopy of solid CO-CO₂ mixtures and layers. *Astron. Astrophys.* 451 (May), 723–731.
- Westley, M.S., Baratta, G.A., Baragiola, R.A., 1998. Density and index of refraction of water ice films vapor deposited at low temperatures. *J. Chem. Phys.* 108 (February), 3321–3326.
- White, D.W., 2010. Laboratory Studies of Solid Carbon Dioxide in Interstellar Ice Analogs Subject to Thermal Processing. Ph.D. Thesis. University of Alabama at Birmingham, CH 310, 1300 University Blvd., Birmingham, AL 35294.
- White, D.W., Gerakines, P.A., Cook, A.M., Whittet, D.C.B., 2009. Laboratory spectra of the CO₂ bending – Mode feature in interstellar ice analogues subject to thermal processing. *Astrophys. J. Suppl. Ser.* 180 (January), 182–191.
- Yue, Y., Angell, C.A., 2004. Clarifying the glass-transition behaviour of water by comparison with hyperquenched inorganic glasses. *Nature* 427 (February), 717–720.